Electrochemical analysis of carbon steel embedded in mortars with pretreated copper tailings as supplementary cementitious material

Carlos Sepúlveda-Vásquez, Nicolás Carrasco-Astudillo, Lisa Muñoz, Paulo Molina, Armelle Ringuedé, Carolina Guerra, Mamié Sancy

International Journal of Electrochemical Science 19 (2024) 100584

Contents lists available at ScienceDirect

International Journal of Electrochemical Science

journal homepage: www.editorialmanager.com/ijoes

Electrochemical analysis of carbon steel embedded in mortars with pretreated copper tailings as supplementary cementitious material

Carlos Sepúlveda-Vásquez [a], Nicolás Carrasco-Astudillo [b], Lisa Muñoz [c], Paulo Molina [d], Armelle Ringuedé [e], Carolina Guerra [f], Mamié Sancy [b,d,g,*]

[a] Departamento de Ingeniería Mecánica y Metalúrgica, Facultad de Ingeniería, Pontificia Universidad Católica de Chile, Santiago 7820436, Chile
[b] Escuela de Construcción Civil, Facultad de Ingeniería, Pontificia Universidad Católica de Chile, Santiago 7820436, Chile
[c] Instituto de Química, Facultad de Ciencias, Pontificia Universidad Católica de Valparaíso, Valparaíso, Chile
[d] Millennium Institute in Green Ammonia, Pontificia, Universidad Católica de Chile, Santiago 7820436, Chile
[e] Chimie ParisTech, PSL Research University, CNRS, Institut de Recherche de Chimie Paris, France
[f] Optics and Photonics Group, Faculty of Engineering, University of Nottingham, University Park, Nottingham NG7 2RD, UK
[g] Center for Research in Nanotechnology and Advanced Materials, Pontificia Universidad Católica de Chile, Pontificia Universidad Católica de Chile, Santiago 7820436, Chile

ARTICLE INFO

Keywords:
Copper tailing
Supplementary cementitious material
Electrochemical behavior
Mechanical properties

ABSTRACT

The cement industry, responsible for 8% of global greenhouse gas emissions, necessitates developing sustainable materials to replace cement partially. This investigation examined the feasibility of using copper tailings, a byproduct of mining, as alternative materials for cement within mortars and reinforced mortars (0–15 wt%). The microstructural composition of the tailings was analyzed using scanning electron microscopy and X-ray diffraction. The corrosion resistance of mortars reinforced with copper tailings was elucidated through open-circuit potential measurements and electrochemical impedance spectroscopy. The results showed that incorporating 5 and 10 wt% of sieved copper tailings improved the mechanical strength and significantly enhanced the electrochemical stability, as indicated by more noble open-circuit potential values. Specifically, the sieved tailings played a crucial role in forming a more stable oxide film, which was confirmed by higher impedance values, suggesting a reduced corrosion rate. In contrast, mortars with 5 wt% of milled tailings exhibited properties like those of the control group. This electrochemical understanding highlights the potential of processed copper tailings in mitigating the environmental impact of cement production and enhancing the durability of cementitious composites.

1. Introduction

The cement industry produces nearly 4 billion tons annually of cement [1,2], which is equivalent to 8% of global carbon dioxide (CO_2) emissions [3], producing 1 ton of CO_2 for every 1 ton of cement [4,5]. It has been proposed that substituting cement with supplementary cementitious materials (SCMs) reduces cement production and associated emissions [6,7]. SCM consists of soluble powders mainly composed of silica, alumina, and calcium oxide [8,9]. The use of SCM contributes to the cement matrix through the effects of (1) pozzolanic and (2) filler [10], improving the mechanical behavior and durability.

The pozzolanic reactions have been related to forming portlandite ($Ca(OH)_2$) and silicates. In this context, it was reported that the replacement of cement by silica fume and metakaolin at 15 wt% reduced by half the water absorption when compared to concrete without replacement at 28 days, also increasing the surface electrical resistance of the concrete from 2.7 to 2.0 times compared to the concrete without replacement. Furthermore, it was reported that adding silica fume and metakaolin improved chloride ion penetration by more than 50% after 28 days, especially when using silica fume [11]. Also, Güneyisi et al. [12] reported that adding metakaolin between 5 and 15 wt% to the mixture increased its compressive strength by approximately 40% after 28 days, attributable to the improved cement paste and aggregate quality. The authors reported that the concrete durability improved due to decreased porosity generated by dense calcium silicate hydrate (C-S-H) production [9].

* Corresponding author at: Escuela de Construcción Civil, Facultad de Ingeniería, Pontificia Universidad Católica de Chile, Santiago 7820436, Chile.
E-mail addresses: cdsepulveda@uc.cl (C. Sepúlveda-Vásquez), mamiesancy@uc.cl, mamiesancy@gmail.com (M. Sancy).

https://doi.org/10.1016/j.ijoes.2024.100584
Received 8 February 2024; Received in revised form 10 April 2024; Accepted 10 April 2024
Available online 16 April 2024

Mining waste, such as copper tailings, has been proposed as an SCM. Copper production is nearly 20.000 tons per year, generating 200 tons of copper tailings per 1 to of refined copper [13]. Copper tailing is composed mainly of Albite (Na,Ca)Al(Si, Al)$_3O_8$), α-quartz (α-SiO_2), Sanidine ($KAlSi_3O_8$), and calcium silicates [14]. Several pre-treatments have been studied for copper tailing as SCM, such as calcination, which has shown better response between 700 and 850 °C. However, this process also generates CO_2 emissions and high energy costs. It is worth mentioning that cement replacement by copper tailing has focused between 0 and 20 wt% due to more significant replacements, which have reduced the mechanical properties and required further pre-treatment, increasing the energy costs. In this context, Onuaguluchi and Eren [15] reported replacing 10 wt% with copper tailings increased concrete compressive strength by 16.2% at 28 days. Dandautiya and Singh [16] studied the combined use of fly ash and copper tailings, finding that the most favorable mixture was using 20 wt% of cement replacement by fly ash and 5 wt% by copper tailings, increasing compressive strength by 8.27% and reducing CO_2 equivalent emissions by 14%. Esmaeili et al. [17,18] studied the replacement of copper tailings from mines in Iran, finding that compressive strength improved with cement replacement of up to 30% at 90 days, associated with the delayed response of the pozzolanic and filler effects, determining the optimal cement replacement to vary between 15 and 20 wt%. However, the SCM must often be pre-treated to optimize its performance through industrial processes involving significant energy costs. For instance, using kaolinite clays requires 10% of the thermal energy to be added as cement replacement [19]. Table 1 shows a resume of the mechanical behavior of different types of SCMs, revealing that industrial wastes, such as fly ash and stainless-steel slag, have better compressive responses than copper tailings, which was related primarily to the water-binder ratios with a similar percentage of cement replacement.

The effect of Cu tailing on corrosion over metallic bars embedded in mortar is currently unknown. Several studies have been conducted on another kind of SCM. For instance, Stefanoni et al. [23] and Hemkemeier et al. [24] have reported a reduction in the corrosion current density (I_{corr}) using fly ash and slag as SCM in reinforced structures. Koga et al. [25] studied the effect of fly ash addition through open-circuit potential (E_{OC}) measurements, reporting a shift of potential towards more positive values in samples with added fly ash, also reaching similar I_{corr} values after 365 days of exposure [26]. Montemor et al. [27] observed an increase in load transfer resistance with 30 wt% fly ash as cement replacement, increasing by a factor of 4 compared to samples without substitution. Zhang et al. [26] investigated copper tailings, proposing that the mortar's quality is the main factor determining the corrosion behavior, reporting matrix failure with replacements above 30 wt%.

This work studied the copper tailing as SCM after a milling treatment as cement replacement between 0% and 15%. Morphological, microstructural, and mechanical behavior of mortars were investigated using scanning electron microscopy, X-ray diffraction, compressive and flexural tests. The corrosion of steel carbon embedded in mortars was also analyzed using electrochemical techniques to understand the effect of the hydration and hardness processes over time.

2. Methodology

2.1. Conditions of copper tailing

The copper tailings were characterized upon receipt and then used as received with particles under the size of 75 μm to replicate the condition of the commercial cement, which has particle size lower than this value [10,28,29]. Vargas et al. [10] characterized the particle size distribution for copper tailings as SCM, obtaining a size lower than 100 μm. Cu tailing was also used after ball milling for 6 h in a ratio of copper tailings/balls of 1:2 with 600 rpm.

2.2. Copper tailing characterization

The chemical composition of the tailings was determined using Energy-Dispersive X-ray Spectroscopy (EDS) on an FE-SEM Model QUANTA 250 FEG. The crystallographic phase composition of the tailings was analyzed qualitatively using X-ray diffraction (XRD) on a Bruker D8 Advance diffractometer operating at 40 kV. Rigaku with a Cu $K_{\alpha 1,2}$; K_β source. The diffractograms were recorded between angles $2\theta = 10^\circ - 80^\circ$, using a scan rate of 0.02 $^\circ \bullet s^{-1}$ at room temperature.

2.3. Sample fabrication

Mortar mixtures were manufactured with Portland cement replacement according to the ASTM C305- 20, using copper tailings as partial cement replacement, between 5 and 15 wt%, as received with particles under the size of 75 μm and milled, as mentioned in Section 2.1. The water/cement (w/c) ratio was 0.5. Portland cement was also used according to ASTM C 595: Type P (Portland-Puzolanic Cement, Melon, Chile) and a commercial fine river sand (Maipo, Chile). Prismatic mortar samples were manufactured to be mechanically tested according to ASTM C109/C109M – 21, with dimensions of 40 mm×40 mm x 160 mm, as shown in Fig. 1(a).

For corrosion analysis, carbon steel bars A630–420 H were used (CAP Acero, Chile) with a nominal composition of (wt%) 0.18–0.44 C, 0.6–1.1 Mn, ≤0.012 P, ≤0.04 S, ≤0.15 Si, and Fe as the balance [30]. The bars were 150 mm long and 15 mm in diameter, which were cleaned through chemical pickling (3 times for 10 min.), drizzled with an anhydrous ethanol solution, and dried with warm air in agreement with ASTM G1. The carbon steel bars without striated were then painted with anticorrosive paint to isolate a specific geometrical area, as shown in Fig. 1(b). After 24 h, the metal samples were embedded in a mortar matrix. Fig. 2 shows an optical microscope image of interface carbon steel - mortar used for electrochemical measurements before exposure.

2.4. Mechanical evaluation

Compressive strength and flexural tests were performed on the prismatic samples after 7, 28, and 90 days of exposure to a saturated solution $Ca(OH)_2$ [31]. A constant velocity of 4 mm$\bullet$min^{-1} in compressive strength and 1 mm$\bullet$min^{-1} in flexural tests was applied

Table 1
Mechanical behavior of replacing different SCMs compared to a mix without replacement at 28 days.

SCMs	Water/Binder Ratio	Cement replacement (wt%)	Compressive Strength at 28 days ($f_{c,28\ days}$) (MPa)	Flexural Strength at 28 days ($f_{c,28\ days}$) (MPa)	References
Copper tailings	0.485	25	9	-	[20]
	0.485	32	8	-	
	0.485	10	26	7.5	
	0.485	15	24	7	
Ground granulated blast furnace slag.	Varied	0–10	63–40	Varied	[20]
Stainless steel slag waste	Varied	10–30	57.37–33.55	Varied	[20]
Fly ash	0.43	25–40	52.2–41.6	Varied	[21,22]
Silica Fume	0.44–0.45	5–10	52.6–57.6	Varied	[21]

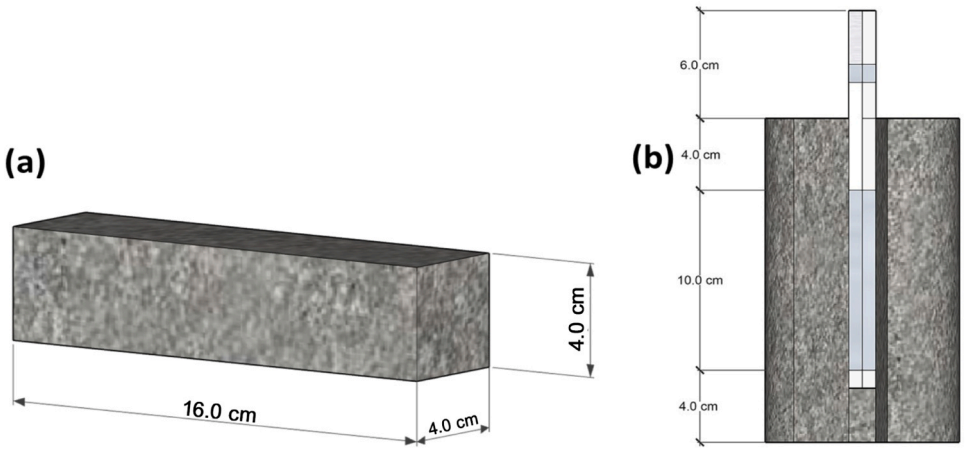

Fig. 1. Scheme representation of samples for (a) mechanical and (b) electrochemical analysis.

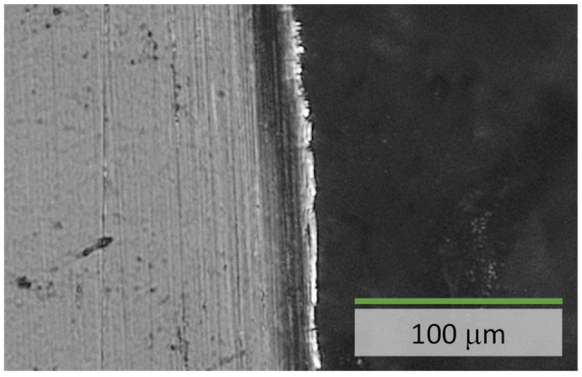

Fig. 2. Optical microscope image of interface carbon steel-mortar before exposure.

using a TC 10001 (homemade), which was done according to standards ASTM C109 – 21 and ASTM C348. All tests were measured in triplicate.

2.5. Thermogravimetry

The mortar samples were analyzed using thermogravimetry measurements after 28 days of hydration, which was halted by immersing in isopropanol using a Setsys Evolution ATG 16/18 easy fit by SETARAM equipment, which was set to stabilize at 40 °C for 20 min. The analysis was performed between 60 °C and 1200 °C using air as the sweep gas, with a heating rate of 10 °C min^{-1}.

2.6. Electrochemical evaluation

The electrochemical tests were measured during 56 days of exposure to a saturated $Ca(OH)_2$ solution at 23 °C [31]. Open circuit potential (E_{OC}), electrochemical impedance spectroscopy (EIS), and linear sweep voltammetry (LSV) measurements were carried out using a potentiostat/galvanostat (Bio-Logic, VSP), a three-electrode electrochemical cell, with graphite and a saturated calomel electrode (SCE) employed as the counter and reference electrodes, respectively. The carbon steel embedded in mortar, described in Section 2.3, was used as the working electrode, with a geometrical exposure area of 45.23 cm^2. EIS data were collected between 65 kHz and 3 mHz, with seven points per decade, using a ±10 mV peak-to-peak sinusoidal voltage at $E = E_{OC}$ and $E = E_{OC}$ ±200 mV. The EIS data were fitted using SIMAD (LISE UPR 15 CNRS, France) between 1 MHz and 1 µHz.

3. Results and discussion

3.1. Copper tailing characterization

Fig. 3 shows the morphology of Cu tailings at different conditions, which reveals a broader particle size distribution for the samples as received and milled (see Fig. 3a,c) than sieved Cu tailings, which have particle size under the size of 75 µm (see Fig. 3b), which was determined using image analysis. The Cu tailing's particle size was slightly more significant than the cement particle size, as reported for SCM particle size by Seraj et al. [29] and Vargas and Lopez [10]. It has been reported that using small particle sizes reduces the permeability, segregation, and attack of concrete sulfates, improving mechanical resistance and durability. The latter was related to the pozzolanic activity in ordinary Portland cement, forming calcium silicate hydrate (C-S-H) of second order [32] due to the presence of Portlandite ($Ca(OH)_2$) in the cement paste. In addition, it has been proposed that smaller particle sizes can benefit the cement hydration kinetic for SCM, improving the mechanical strength. However, the viscosity can also increase, reducing the workability [33,34].

Table 2 shows the chemical composition of Cu tailing obtained by XRD analyses, revealing that Si, Ca, and Al are the main chemical elements, forming different compounds, such as Albinite ((Na, Ca)Al(Si, $Al)_3O_8$) and a-quartz low (α-SiO_2), as main compounds in sieved and milled Cu tailing. For sieved Cu tailings, XRD analysis revealed the presence of Sanidine ($KAlSi_3O_8$) and other calcium aluminum silicates, such as 1.7 wt% Gehlenite ($Ca_2Al(SiAl)O_7$) 1.2 wt% Gmelinite ($(Ca_2K_4Na_4)(Si_8Al_4)O_{24}x11H_2O$. For milled Cu tailings, XRD analysis also revealed the formation of quartz (SiO_2).

Fig. 4 shows the XRD patterns of copper tailing as received and milled, revealing the presence of Albite and α-quartz low for both samples, as reported by Qing et al. [35,36]. It is well known that the presence of α-quartz low in OPC influences the cement hydration and pozzolanic activity [37]. A reduction in pozzolanic activity was reported due to the presence of Albite and Sanidine [38]. In this case, the presence of Gehlenite and Gmelinite in the sieved Cu tailings and the trigonal structure of quartz in the milled Cu tailings could improve the pozzolanic activity [39], which could also play an essential role in the hydration of the mortar, consequently, in the mechanical properties.

The Cu tailing was also analyzed using X-ray fluorescence, determining that Fe, S, K, Ca, Cu, Pb, and Cd are permissible values according to Standard 503–40 CFR/1993 [40] and Australian Standard AS 4454–1999 [41], as previously reported by our group. These concentration values are similar to those found by other research groups [14, 18,42]. Therefore, copper tailing does not present harmful amounts for use as SCM.

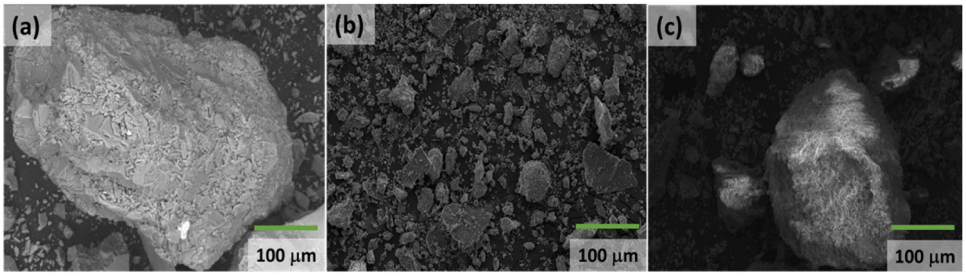

Fig. 3. FE-SEM images of Cu tailing. (a) As received, (b) sieved under 75 µm, and (c) milled as pre-treatment.

Table 2
Chemical composition (in wt%) analysis of copper tailing obtained by XRD analyses.

Sample	Albite	α-quartz low	Sanidine	quartz	Others
Sieved	57.3	30.7	9.1		2.9
Milled	50.5	25.2	-	24.3	-

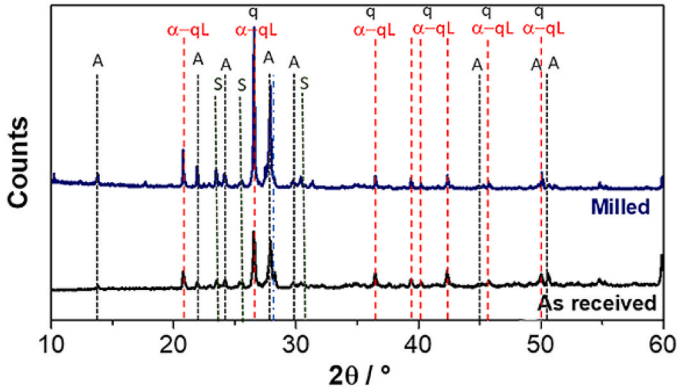

Fig. 4. X-ray pattern of Cu tailing as received (low) and milled (up).

3.2. Mechanical mortars analysis

Fig. 5 shows the samples' compression strength (f_c) as a function of exposure time and cement replacement of Cu tailing sieved and milled. Both graphs reveal an enhancement by adding 5 and 10 wt% sieved Cu tailings over time, which is even more significant than control mortar without replacement. However, incorporating milled Cu tailings decreased the compression strength, except using 5 wt% of milled Cu tailing after 90 days of exposure, suggesting that the milled Cu tailing can delay the hydration reactions in mortars. In all cases, it is observed that the mortar strengthening is adversely affected as the replacement percentage increases. Fig. 5(a) shows that after 90 days of maturation, the mortar with 5 wt% Cu tailing can reach 38 MPa while the control comes to 31 MPa, demonstrating that Cu tailing with small particles is suitable from a mechanical point of view. Onuaguluchi and Eren [15] reported increased compressive strength, adding 10 wt% of Cu tailings to concrete after 28 days, using 50% of particle size was lower than 0.1 mm. Dandautiya and Singh [16] determined that the compressive strength improved by incorporating 20 wt% of fly ash and 5 wt% of Cu tailings without any pre-treatment by the SCM. Esmaeili et al. [17,18] also reported better compressive strength using 15–20 wt% of Cu tailings after 90 days, which was milled for 3 h at 300 rpm to reach particle size finer than 45 µm for the 98%.

Fig. 6 shows samples' flexion strength (f_m) as a function of exposure time and cement replacement, revealing an improvement using sieved Cu tailing compared with the milled treated, which is more drastic for more prolonged exposure. However, no clear trend was observed for milled samples, and better results were found for longer exposure time. Vargas et al. [43] analyzed the pre-treatment of Cu tailing as SCM by a modeling approach, reporting an enhancement of the mechanical behavior on the concrete mixture by adding 20 wt% of Cu tailings thermally treated [44].

3.3. Thermogravimetry

Fig. 7 shows the thermogravimetric analysis of the mortars with different replacements after 28 days, revealing thermal zones related to (I) gypsum dehydrated at below 150 °C, (II) Portlandite ($Ca(OH)_2$) dehydroxylates ($Ca(OH)_2 \rightarrow CaO + H_2O$) between 400 and 600 °C, and (III) Calcium carbonate ($CaCO_3$) decomposes above 600°C to CaO and CO_2, as previously reported by Lothenbach et al. [45]. Also, Fig. 7 shows that the first thermal step between room temperature and 150 °C was reduced by adding 5 wt% of sieved Cu tailing. A similar peak is observed for samples with 5 and 15 wt% milled Cu tailings. Madali and Wei [46]

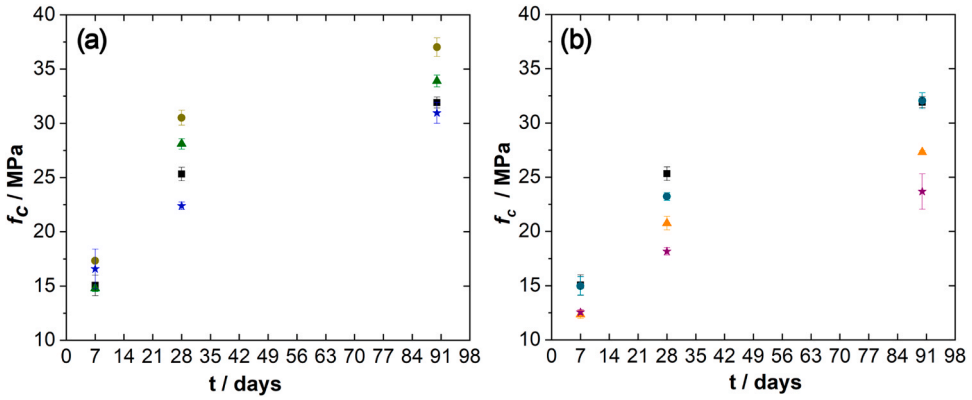

Fig. 5. Maximum compressive strength of mortars with different cement replacements after exposure to saturated $Ca(OH)_2$ solution at room temperature. (■) 0 wt%, (●) 5 wt%, (▲) 10 wt%, (★) 15 wt% of cement replacement.

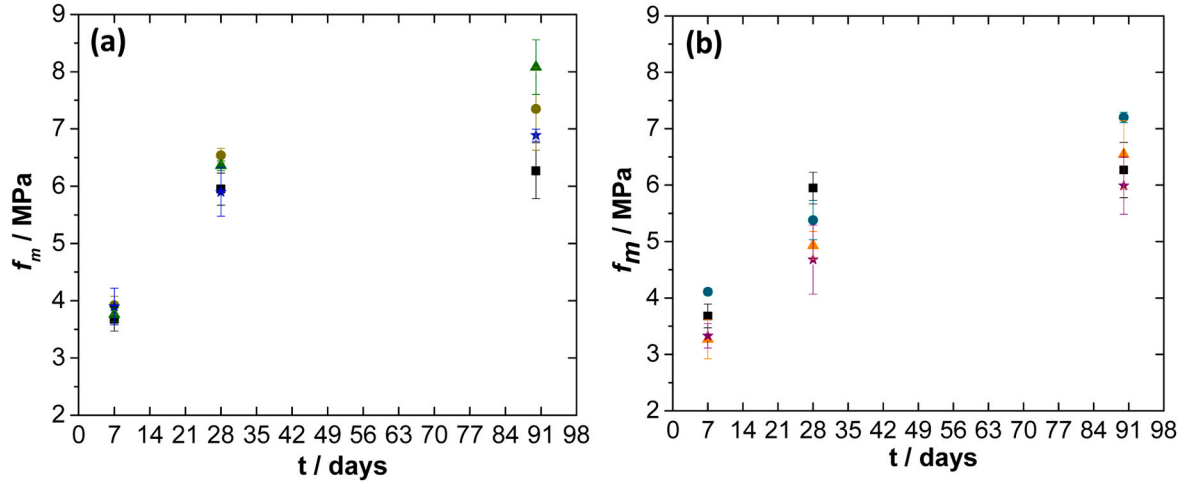

Fig. 6. Maximum flexion strength of mortars with different cement replacements after exposure to saturated $Ca(OH)_2$ solution at room temperature. (a) Sieved to particle size < 75 μm and (b) milled Cu tailings. (■) 0 wt%, (●) 5 wt%, (▲) 10 wt%, (★) 15 wt% of cement replacement.

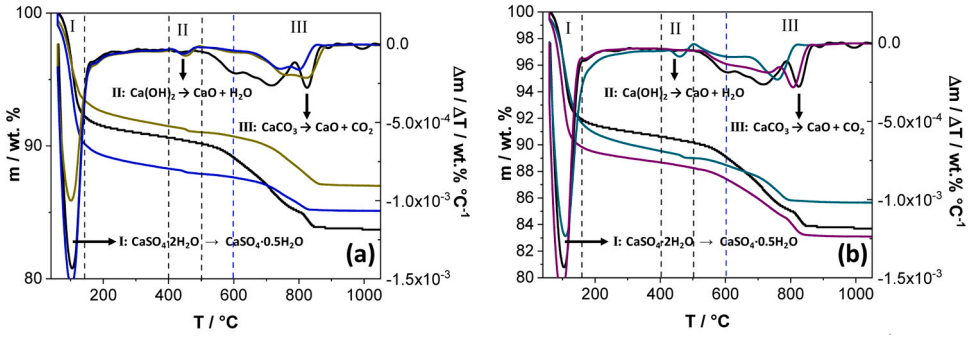

Fig. 7. The effect of Cu tailings replacement on the thermogravimetric analysis of the mortars after 28 days. (a) Sieved to particle size <75 μm and (b) milled Cu tailings. (—) 0 wt%, (—, —) 5 wt.%, and (—, —) 15 wt% of cement replacement.

related this step thermal to the evaporation of the adsorbed and interlayer water (30–109 °C) and dehydration of C-S-H [45]. However, a step thermal at 130 °C was previously attributed to the dehydration of Ettringite and gypsum [47], as described by Katsioti et al. [48]. Additionally, the incorporation of 5 wt% of sieved Cu tailings and 15 wt% of milled Cu tailings increased the peak at 450 °C, which was associated with the Portlandite dehydroxylates ($Ca(OH)_2$) [45,48]. A few dehydration products were formed by adding 15 wt% of Cu tailing, as sieved and milled.

3.4. Electrochemical behavior of carbon steel embedded in mortars

Fig. 8 shows the evolution of the carbon steel bar's open circuit potential (E_{oc}) embedded in the mortar through exposure, with different cement replacement percentages. As can be seen, the E_{oc} was shifted to more positive values at earlier stages, which was more drastic for sieved samples than milled samples, suggesting a slight improvement in the protection of the steel bar, according to the ASTM C876 standard [49]. All samples reached a more stable E_{oc} value between −200 mV and

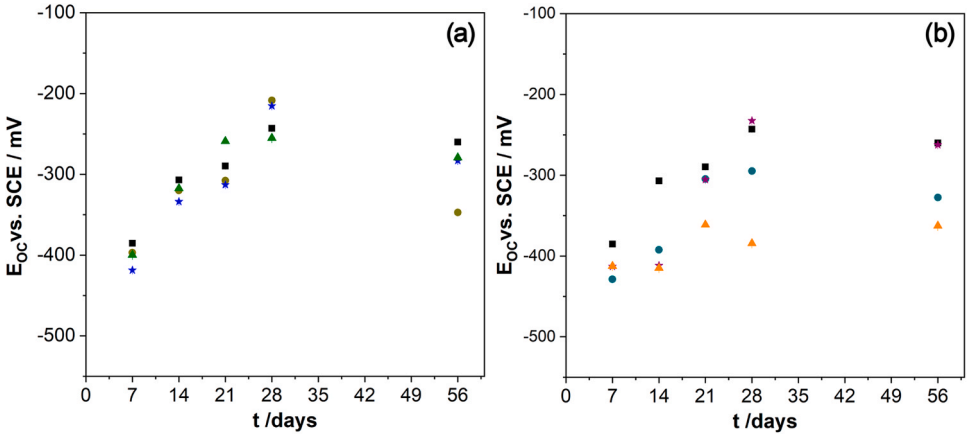

Fig. 8. Open circuit potential of carbon steel embedded in mortars after 56 days of exposure to $Ca(OH)_{2,sat}$ at room temperature with different cement replacements by Cu tailing over time. (a) Sieved to particle size <75 μm and (b) milled Cu tailings. (■) 0 wt%, (●) 5 wt%, (▲) 10 wt%, (★) 15 wt% of cement replacement.

−300 mV for longer exposure time. Fig. 7 shows the E_{oc} values with their standard deviation, which had excellent reproducibility. Stefanoni et al. [23] proposed that the more negative potentials of the metallic bar embedded in carbonated concrete were associated with a high corrosion rate. Hemkemeier et al. [24] reported a shift in the E_{oc} values using industrial wastes in cementitious composites, which was attributed to the wetting/drying cycles, increasing the porosity.

Fig. 9 shows the Nyquist diagrams, at different frequency ranges, of reinforced mortar samples after exposure at $E=E_{oc}$ as a representative example of studied systems, revealing two capacitive loops superimposed, one of them at very high-frequency ranges (HF), between 65 kHz and 100 Hz, and another between medium and low-frequency ranges (MF-LF), between 100 Hz and3 mHz. Fig. 9(a) shows the impedance response at the whole frequency range with slight differences between samples between HF and LF ranges. Fig. 9(b) shows a zoom of the VHF, revealing a shift of the real part of the impedance with 10 wt% and 15 wt% of cement replacement concerning the control specimens. Fig. 9(c) shows the experimental and simulated impedance data.

Novoa et al. [50,51] proposed that the impedance response at VHF can be related to the porosity, pore size distribution, and dielectric properties of cementitious cover. Therefore, the changes produced at VHF could be provoked by the cement replacement, which modified the mortar bulk morphology, as was demonstrated by the compressive strength. Fig. 9(c) shows the Nyquist diagrams between MF-LF, which is associated with the response of the carbon steel bars embedded in the cementitious matrix, clearly revealing the changes between samples. Meyer et al. [52] related the impedance response of reinforced concretes to the porous electrode behavior, reporting two-time constants.

Fig. 10 shows the Nyquist diagrams of reinforced mortar samples without partial cement replacement after 28 days of exposure, comparing the impedance response at open circuit potential ($E=E_{oc}$) with cathodic and anodic overpotentials ($E=E_{OC}\pm200$ mV). No significant differences are observed, suggesting that the impedance response at $E=E_{oc}$ is under mixed control between the anodic and cathodic reactions.

Fig. 11 shows the equivalent circuits proposed for reinforced mortar samples after exposure, based on that proposed by Novoa et al. [50] for the range VHF to MF and for the range MF to LF based on that proposed by Shi et. al, [53], Shi et al. [54] and Feng et al. [55], where R_{PP} represents the percolating pore resistance, which is interconnected pores, and in parallel is R_{OP} corresponds to the occluded pore resistance. In this case, non-ideal capacitances were included for the bulk part and occluded in mortar parts, which were expressed by a constant phase element (CPE) [56,57] by Q coefficient and α□ Therefore, Q_{bulk},α_{bulk}, and Q_{OP},α_{OP}, respectively. The experimental impedance data at VHF,

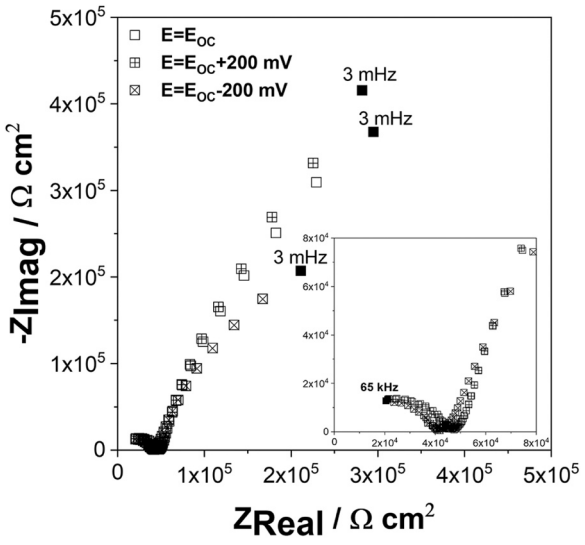

Fig. 10. Nyquist diagrams of carbon steel embedded in mortar samples without Cu tailing addition after 28 days of exposure to $Ca(OH)_{2,sat}$ solution after 28 days at (□) $E = E_{OC}$, (x) $E = E_{OC}$ +200 mV, and (+) $E = E_{OC}$-200 mV.

collected between 65 kHz and 100 Hz, were adjusted and simulated between 40 MHz and 100 Hz, as shown in Fig. 8(b). In addition, R_{oxide} represents the oxide resistance, $R_{ct,a}$ is the anodic charge transfer resistance, CPE_{oxide} corresponds to the oxide capacitance, and CPE_{dl} is the double-layer pseudo-capacitance.

Fig. 12 shows the evolution of the CPE parameters of the bulk cementitious part as a function of exposure time, revealing that the Q_{bulk} values decreased drastically up to 24 h, from 10^{-6} to 10^{-10} $F•s^{(\alpha-1)}•cm^{-2}$, with higher variation for sieved than milled samples, possibly due to the hydration reactions in mortars. Later, the Q_{bulk} coefficient reached more stable values, around 10^{-10} to 10^{-9} $F•s^{(\alpha-1)}•cm^{-2}$ for both samples. It should be noted that using 15 wt% of sieved Cu tailing, the Q_{bulk} coefficient did not vary dramatically during the exposure.

Liu et al. [58] reported Q values slightly higher using basalt fiber as a new anti-corrosion for steel bars in reinforced concrete, which is environmentally friendly and improves the durability of samples. Meyer et al. [52] studied the corrosion behavior of embedded steel bars into concretes, estimating Q values for the concrete parts that varied between 10^{-12} to 10^{-9} $F•cm^{-2}$ between 7 and 28 days of exposure. Fig. 12 also shows the variation of α related to the bulk cementitious part as a

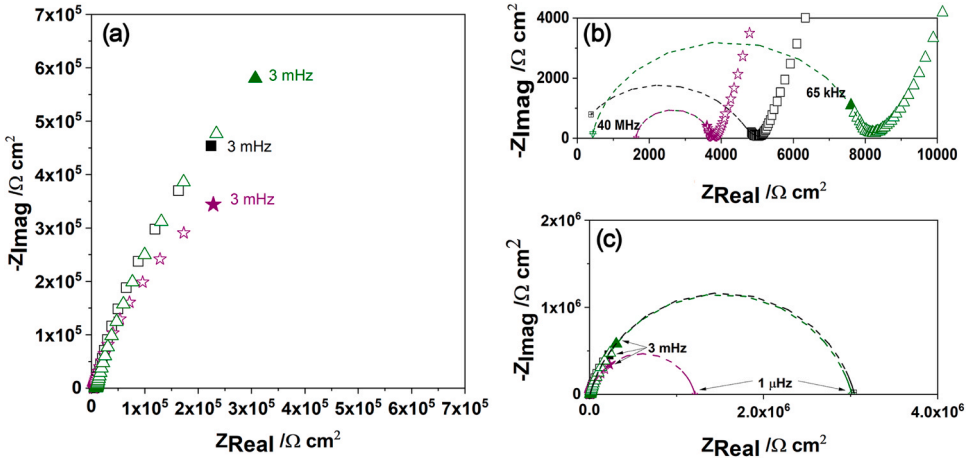

Fig. 9. Nyquist diagrams of carbon steel embedded in mortar samples after 28 of exposure to $Ca(OH)_{2,\ sat}$ at room temperature, and $E = E_{OC}$. (a) all frequency range, (b) VHF, and (c) HF to LF range. (■) 0 wt%, (▲) 10 wt%, (★) 15 wt% of Cu tailings. (–) Simulated impedance data.

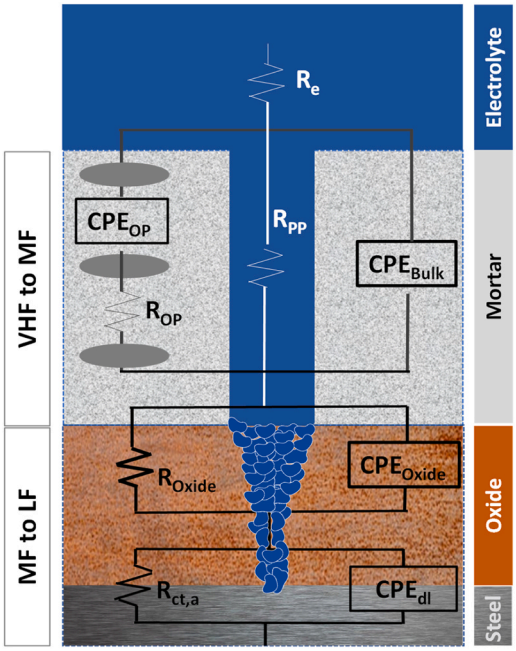

Fig. 11. A proposed equivalent circuit for carbon steel embedded in mortars after $Ca(OH)_2$ exposure at $E=E_{OC}$.

function of exposure time, revealing a drastic increase up to 28 days, from 0.5 to 0.9 approximately, keeping constant close to 0.9, which can be related to an evolution of the hydration process more homogenous. Andrade et al. [59] proposed that the morphological changes in mortars and concretes can be attributed to the structure's durability related to changes in porosity and conductivity.

Fig. 13 shows the evolution of the percolating and occluded pores resistances (R_{PP}, R_{OP}) as a function of exposure time, revealing that the R_{PP} increased up to 28 days, from 10^3 to 10^5 Ω•cm^2, which was more significant for sieved samples than milled samples. It should be noticed that for sieved samples, the R_{PP} increased more dramatically as the cement replacement increased. However, R_{PP} was not influenced significantly by adding Cu tailing for milled samples, suggesting that the filler effect was determined by the particle size of the SCM and its distribution. Fig. 13(c,d) shows that R_{OP} increased during exposure, from 10^3 to 10^5 Ω•cm^2, revealing again a more significant effect applying sieved than milled as pre-treatment for Cu tailings, suggesting an influence of the surface area on the pozzolanic activity of Cu tailings as SCM. R_{OP} of sieved Cu tailing is increasing in value compared to the control sample as the replacement rises, demonstrating a decrease in the quantity of occluded porous due to the filled effect of sieved Cu tailing. Instead, the R_{OP} of Cu milled tailing showed similar values to the control sample, which reveals that the pretreatment provokes a change in the crystallinity of some species, observed in the increase of peaks in the X-ray diffraction (XRD), as shown in Fig. 4, which loses its pozzolanic effect compared to sieved tailing.

As mentioned above, the impedance data of carbon steel bars embedded in mortars in MF and LF ranges were measured between 100 Hz to 3 mHz, which were adjusted using the equivalent circuit shown in Fig. 11 [51,59,60]. CPE parameters were used to replace the pure capacitance, as proposed by Gonzalez et al. [61] and Liu et al. [62]. Impedance data were also simulated, reaching frequency values close to 10^{-6} Hz, as shown in Figs. 9(c) and 14, showing the experimental impedance data as symbols and simulated data as lines. Fig. 14(a) reveals that the impedance modulus was influenced by incorporating Cu tailings at the MF to LF range, showing lower values using sieved samples with 15 wt% of cement replacement. Moreover, Fig. 14(b) shows that the corrected phase was close to 75° between 10^{-2} and 10^1 Hz for all samples, which was attributed to a CPE behavior possibly due to the formation of an oxide layer on the steel bars, which is n. The significant effect of the electrolyte correction on Bode plots can be associated with

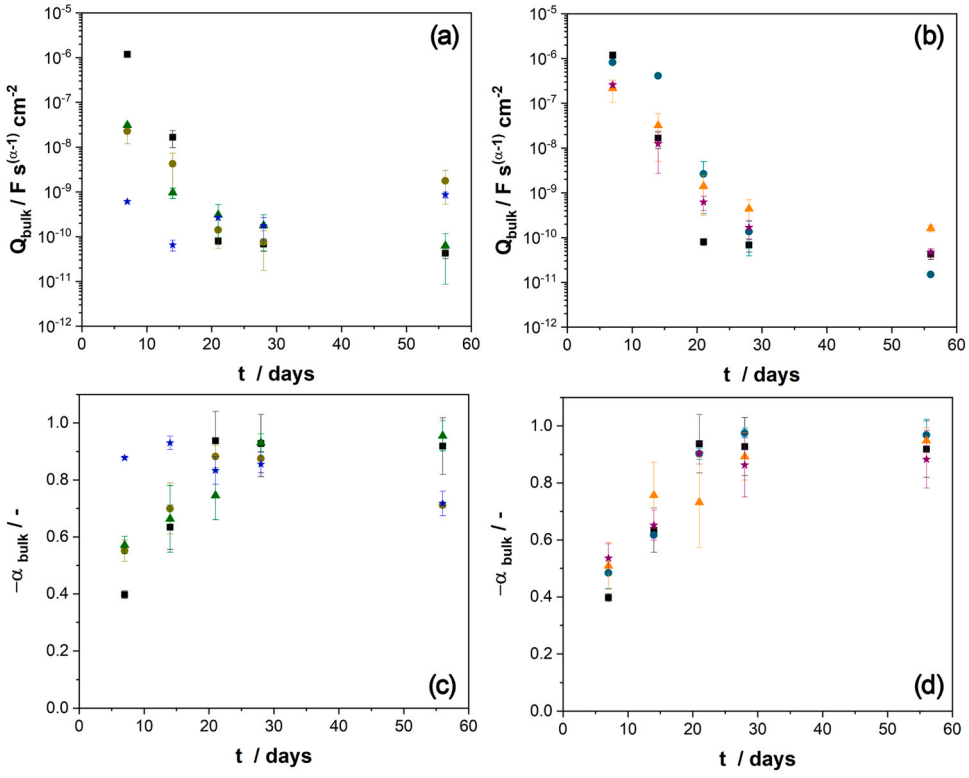

Fig. 12. Constant phase element parameters related to carbon steel's bulk cementitious part mortar embedded in mortars after $Ca(OH)_{2,sat}$ exposure at T_{amb} and $E=E_{oc}$. (a,c) Sieved to particle size < 75 μm and (b,d) milled Cu tailings. (■) 0 wt%, (●) 5 wt%, (▲) 10 wt%, (★) 15 wt% of cement replacement.

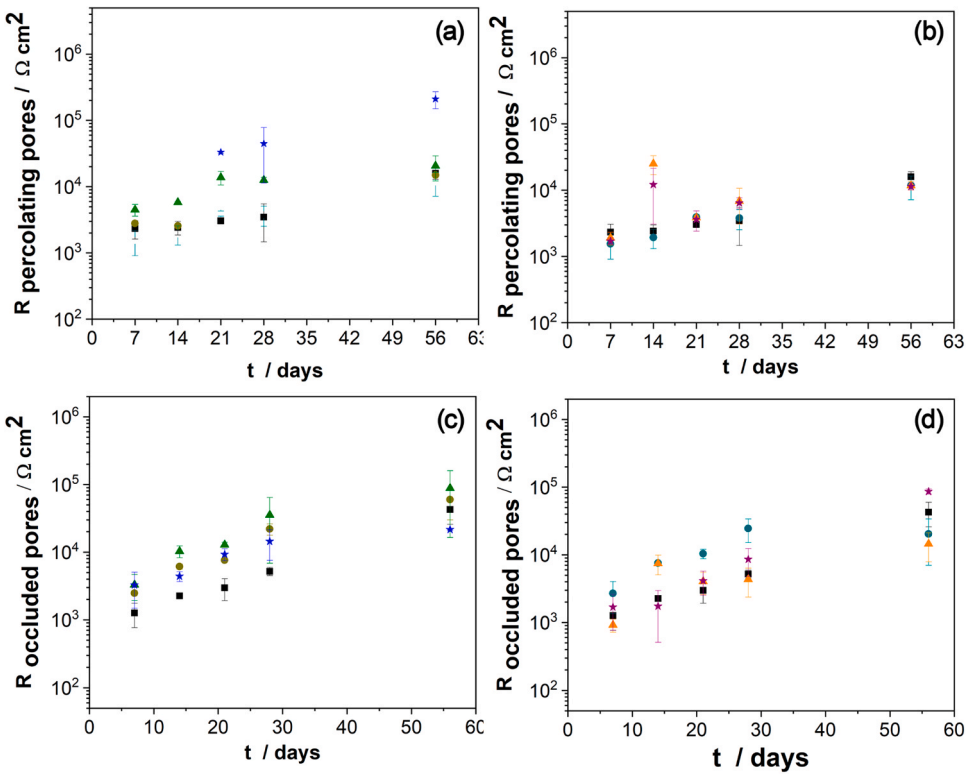

Fig. 13. Effect of copper tailings replacement on the (a,b) percolating pore and (c,d) occluded pore resistance of carbon steel embedded in mortars after $Ca(OH)_{2,\ sat}$ exposure at room temperature. (a,c) Sieved to particle size < 75 μm and (b,d) milled Cu tailings. (■) 0 wt%, (●) 5 wt%, (▲) 10 wt%, (★) 15 wt% of cement replacement.

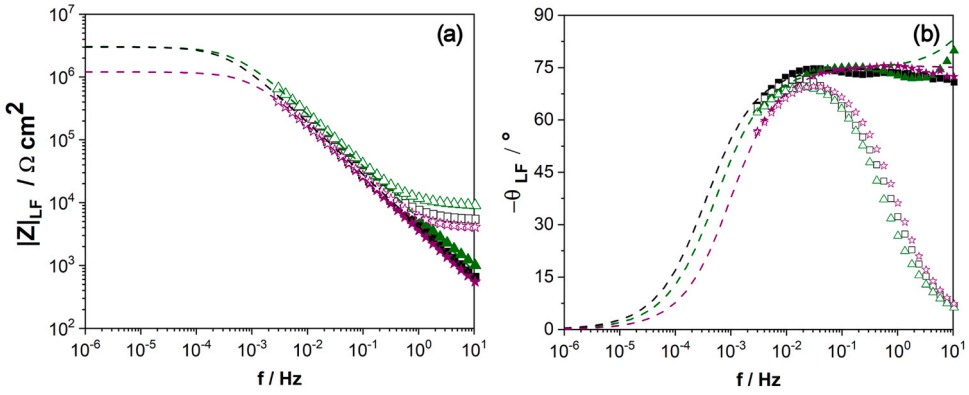

Fig. 14. Bode plots corrected by the electrolyte resistance of carbon steel embedded in mortar after 28 days of exposure to saturated $Ca(OH)_2$ solution at $E = E_{OC}$. (a) Modulus and (b) phase as a function of frequency range. (–) Simulated data at the LF range. (■) 0 wt%, (▲) sieved 10 wt%, and (★) milled 15 wt% of cement replacement.

the geometrical effect of the electrochemical cell used for this kind of system.

Fig. 15 shows the variation of the impedance modulus obtained from the simulated impedance data between medium and low frequency, 10^{-4} and 10^{-6} Hz ($|Z|_{MF\ to\ LF}$), revealing an increase up 28 days of exposure in the control sample but also with sample with its thickness and passive properties up to 28 days, but decreased after 28 days. Therefore, a continuous oxide film formation/dissolution mechanism can be developed in this system. It is worth mentioning that the sample with sieved Cu tailings reached similar $|Z|_{LF}$ values for more prolonged exposure, possibly related to the reduction of the hydration reaction rate. In addition, *a* much better reproducibility is observed using sieved Cu tailing than milled, suggesting *a* more stable oxide film formed in samples using sieved Cu tailing than milled.

Fig. 16 shows the evolution of the R_{oxide} determined from the impedance fit parameters. Adding milled Cu tailing increased R_{oxide} more significantly than the control sample and sieved Cu tailings. However, a reduction of R_{oxide} was determined using cement replacement after 56 days, suggesting that the Cu tailings can temporarily increase the oxide conductivity. Shi et al. [54] and Feng et al. [55] reported R_{oxide} values slightly lower values for this kind of system in marine media, close to 10^5 Ω cm^2, which also increased over time.

4. Conclusion

Mortar and reinforced mortar specimens were prepared using copper tailings contents to evaluate their suitability as supplementary cementitious materials, analyzing the mechanical and electrochemical effects.

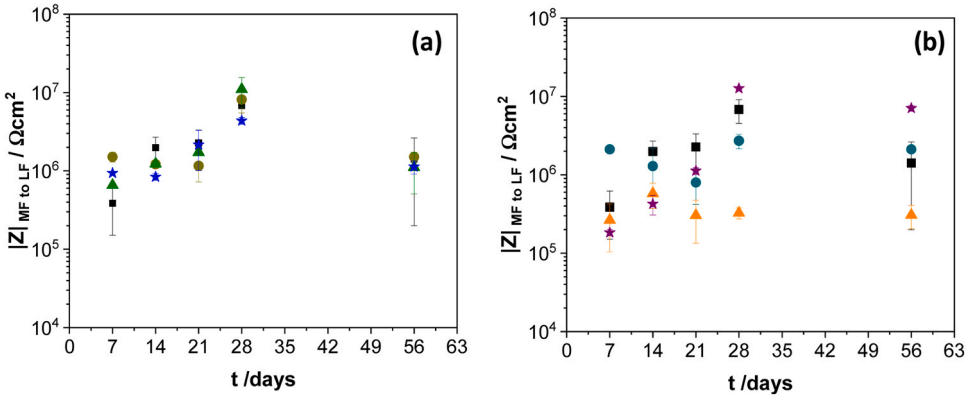

Fig. 15. The effect of cement replacement on the impedance fit module between medium and low frequency of carbon steel embedded mortars in the MF to LF range. (a) Sieved to particle size < 75 μm and (b) milled Cu tailings. (■) 0 wt%, (●) 5 wt%, (▲) 10 wt%, (★) 15 wt% of cement replacement.

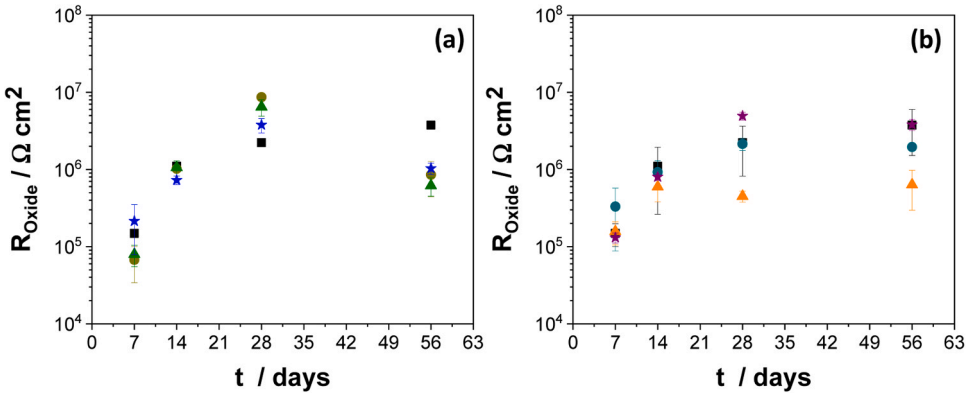

Fig. 16. The effect of Cu tailings as cement replacement on oxide resistance of carbon steel embedded mortars after $Ca(OH)_{2,\ sat}$ exposure at T_{room}. (a) Sieved to particle size < 75 μm and (b) milled. ■) 0 wt%, (●) 5 wt%, (▲) 10 wt%, (★) 15 wt% of cement replacement.

The results allowed us to conclude that Cu tailing in as received condition but with small particles has an adequate pozzolanic capacity. However, a critical cement replacement would be close to 10 wt%. This conclusion is based on:

(1) The mechanical strengthening response was enhanced when Cu tailing was sieved in contrast with a control mortar. However, when Cu tailing is milled, it demonstrates a loosening of its strengthening properties.
(2) A pretreatment such as milling for Cu tailing reduced its pozzolanic properties due to an increase in the crystallinity of the SiO_2, which resulted in a poor reaction during the mortar's maturity.
(3) The electrochemical response of carbon steel embedded in mortars revealed that samples with Cu tailing as cement replacement can reach similar corrosion properties after more prolonged exposure.

Declaration of Competing Interest

The authors declare the following financial interests/personal relationships which may be considered as potential competing interests. Carlos Sepulveda-Vasquez reports financial support was provided by National Agency for Research and Development. If there are other authors, they declare that they have no known competing financial interests or personal relationships that could have appeared to influence the work reported in this paper.

Acknowledgments

The authors would like to thank ANID PFCHA/Doctorado Becas Chile/2019 (Grant 21190220) and Postdoctoral N°3210432, Fondequip (EQM 160091 and 150101), and Millennium Institute on Green Ammonia (Grant ICN2021_023).

References

[1] Z. Cao, L. Shen, J. Zhao, L. Liu, S. Zhong, Y. Sun, Y. Yang, Toward a better practice for estimating the CO2 emission factors of cement production: An experience from China, J. Clean. Prod. 139 (2016) 527–539, https://doi.org/10.1016/j.jclepro.2016.08.070.
[2] A. Mehenni, O. Cuisinier, F. Masrouri, Impact of lime, cement, and clay treatments on the internal erosion of compacted soils, J. Mater. Civ. Eng. 28 (2016) 04016071, https://doi.org/10.1061/(asce)mt.1943-5533.0001573.
[3] R. Kajaste, M. Hurme, Cement industry greenhouse gas emissions - Management options and abatement cost, J. Clean. Prod. 112 (2016) 4041–4052, https://doi.org/10.1016/j.jclepro.2015.07.055.
[4] J. Lehne, and F. Preston, Making Concrete Change Innovation in Low-carbon Cement and Concrete The Royal Institute of International Affairs, Chatham House Report Series, www.chathamhouse.org/sites/default/files/publications/research/2018-06-13-makingconcrete- c, (2018) 138. www.chathamhouse.org.
[5] F. Pacheco Torgal, S. Miraldo, J.A. Labrincha, and J. De Brito, An overview on concrete carbonation in the context of eco-efficient construction: Evaluation, use of SCMs and/or RAC, (2012). doi:10.1016/j.conbuildmat.2012.04.066.
[6] A. Hasanbeigi, L. Price, E. Lin, Emerging energy-efficiency and CO 2 emission-reduction technologies for cement and concrete production: a technical review, Renew. Sustain. Energy Rev. 16 (2012) 6220–6238, https://doi.org/10.1016/j.rser.2012.07.019.
[7] I. Petersson, M. Lilja, J. Hammel, A. Kottorp, Impact of home modification services on ability in everyday life for people ageing with disabilities, J. Rehabil. Med. 40 (2008) 253–260, https://doi.org/10.2340/16501977-0160.

[8] M.C.G. Juenger, R. Snellings, S.A. Bernal, Supplementary cementitious materials: new sources, characterization, and performance insights, Cem. Concr. Res 122 (2019) 257–273, https://doi.org/10.1016/j.cemconres.2019.05.008.
[9] M.C.G. Juenger, R. Siddique, Recent advances in understanding the role of supplementary cementitious materials in concrete, Cem. Concr. Res 78 (2015) 71–80, https://doi.org/10.1016/j.cemconres.2015.03.018.
[10] F. Vargas, M. Lopez, Development of a new supplementary cementitious material from the activation of copper tailings: mechanical performance and analysis of factors, J. Clean. Prod. 182 (2018) 427–436, https://doi.org/10.1016/j.jclepro.2018.01.223.
[11] A. Borosnyói, Long term durability performance and mechanical properties of high performance concretes with combined use of supplementary cementing materials, Constr. Build. Mater. 112 (2016) 307–324, https://doi.org/10.1016/J.CONBUILDMAT.2016.02.224.
[12] E. Güneyisi, M. Gesoğlu, S. Karaoğlu, K. Mermerdaş, Strength, permeability and shrinkage cracking of silica fume and metakaolin concretes, Constr. Build. Mater. 34 (2012) 120–130, https://doi.org/10.1016/j.conbuildmat.2012.02.017.
[13] G. Bridge, The social regulation of resource access and environmental impact: production, nature and contradiction in the US copper industry, (n.d.). www.elsevier.com/locate/geoforum (accessed March 11, 2024).
[14] C. Sepúlveda-Vásquez, N. Carrasco-Astudillo, L. Muñoz, C. Guerra, and M. Sancy, Electrochemical analysis of the effect of copper tailings on mortars, 2024.
[15] O. Onuaguluchi, Ö. Eren, Rheology, strength and durability properties of mortars containing copper tailings as a cement replacement material, Eur. J. Environ. Civ. Eng. 17 (2013) 19–31, https://doi.org/10.1080/19648189.2012.699708.
[16] R. Dandautiya, A.P. Singh, Utilization potential of fly ash and copper tailings in concrete as partial replacement of cement along with life cycle assessment, Waste Manag. 99 (2019) 90–101, https://doi.org/10.1016/J.WASMAN.2019.08.036.
[17] J. Esmaeili, H. Aslani, Use of copper mine tailing in concrete: strength characteristics and durability performance, J. Mater. Cycles Waste Manag 21 (2019) 729–741, https://doi.org/10.1007/s10163-019-00831-7.
[18] J. Esmaeili, H. Aslani, O. Onuaguluchi, Reuse potentials of copper mine tailings in mortar and concrete composites, J. Mater. Civ. Eng. 32 (2020) 04020084, https://doi.org/10.1061/(ASCE)MT.1943-5533.0003145.
[19] M.U. Hossain, C.S. Poon, Y.H. Dong, D. Xuan, Evaluation of environmental impact distribution methods for supplementary cementitious materials, Renew. Sustain. Energy Rev. 82 (2018) 597–608, https://doi.org/10.1016/j.rser.2017.09.048.
[20] C.J. Tsai, R. Huang, W.T. Lin, H.N. Wang, Mechanical and cementitious characteristics of ground granulated blast furnace slag and basic oxygen furnace slag blended mortar, Mater. Des. 60 (2014) 267–273, https://doi.org/10.1016/J.MATDES.2014.04.002.
[21] A. Mardani-Aghabaglou, G. Inan Sezer, K. Ramyar, Comparison of fly ash, silica fume and metakaolin from mechanical properties and durability performance of mortar mixtures view point, Constr. Build. Mater. 70 (2014) 17–25, https://doi.org/10.1016/J.CONBUILDMAT.2014.07.089.
[22] A. Benli, M. Karataş, Y. Bakir, An experimental study of different curing regimes on the mechanical properties and sorptivity of self-compacting mortars with fly ash and silica fume, Constr. Build. Mater. 144 (2017) 552–562, https://doi.org/10.1016/J.CONBUILDMAT.2017.03.228.
[23] M. Stefanoni, U. Angst, B. Elsener, Corrosion rate of carbon steel in carbonated concrete – A critical review, Cem. Concr. Res 103 (2018) 35–48, https://doi.org/10.1016/j.cemconres.2017.10.007.
[24] T.A. Hemkemeier, F.C.R. Almeida, A. Sales, A.J. Klemm, Corrosion monitoring by open circuit potential in steel reinforcements embedded in cementitious composites with industrial wastes, Case Stud. Constr. Mater. 16 (2022), https://doi.org/10.1016/j.cscm.2022.e01042.
[25] G.Y. Koga, B. Albert, V. Roche, R.P. Nogueira, A comparative study of mild steel passivation embedded in Belite-Ye'elimite-Ferrite and Porland cement mortars, Electro Acta 261 (2018) 66–77, https://doi.org/10.1016/J.ELECTACTA.2017.12.128.
[26] L. Zhang, J. Li, H. Qiao, Effect of copper tailing content on corrosion resistance of steel reinforcement in a Salt Lake environment, Materials 12 (2019), https://doi.org/10.3390/MA12193069.
[27] M.F. Montemor, A.M.P. Simões, M.M. Salta, Effect of fly ash on concrete reinforcement corrosion studied by EIS, Cem. Concr. Compos 22 (2000) 175–185, https://doi.org/10.1016/S0958-9465(00)00003-2.
[28] H. Moosberg-Bustnes, B. Lagerblad, and E. Forssberg, The function of fillers in concrete, 2004.
[29] S. Seraj, R.D. Ferron, M.C.G. Juenger, Calcining natural zeolites to improve their effect on cementitious mixture workability, Cem. Concr. Res. 85 (2016) 102–110, https://doi.org/10.1016/j.cemconres.2016.04.002.
[30] F.M.G. Madrid, A. Soliz, L. Cáceres, S. Salazar-Avalos, D. Guzmán, E. Gálvez, Corrosion of Reinforced A630–420 H steel in direct contact with NaCl Solution, Materials 16 (2023) 6017, https://doi.org/10.3390/ma16176017.
[31] M. Chen, H. Yuan, X. Qin, Y. Wang, H. Zheng, L. Yu, Y. Cai, Q. feng Liu, G. Liu, W. Li, Improve corrosion resistance of steel bars in simulated concrete pore solution by the addition of EDTA intercalated CaAl-LDH, Corros. Sci. 226 (2024), https://doi.org/10.1016/j.corsci.2023.111636.
[32] F. Pacheco Torgal, S. Miraldo, J.A. Labrincha, and J. De Brito, An overview on concrete carbonation in the context of eco-efficient construction: Evaluation, use of SCMs and/or RAC, (2012). doi:10.1016/j.conbuildmat.2012.04.066.
[33] X. Sun, J. Liu, Y. Zhao, J. Zhao, Z. Li, Y. Sun, J. Qiu, P. Zheng, Mechanical activation of steel slag to prepare supplementary cementitious materials: a comparative research based on the particle size distribution, hydration, toxicity assessment and carbon dioxide emission, J. Build. Eng. 60 (2022), https://doi.org/10.1016/j.jobe.2022.105200.
[34] B. Ayati, D. Newport, H. Wong, C. Cheeseman, Low-carbon cements: potential for low-grade calcined clays to form supplementary cementitious materials, Clean. Mater. 5 (2022) 100099, https://doi.org/10.1016/j.clema.2022.100099.
[35] L. Qing, S. Shaokang, J. Zhen, W. Junxiang, L. Xianjun, Effect of CaO on hydration properties of one-part alkali-activated material prepared from tailings through alkaline hydrothermal activation, Constr. Build. Mater. 308 (2021), https://doi.org/10.1016/j.conbuildmat.2021.124931.
[36] S. Mabroum, S. Moukannaa, A. El Machi, Y. Taha, M. Benzaazoua, R. Hakkou, Mine wastes based geopolymers: a critical review, Clean. Eng. Technol. 1 (2020), https://doi.org/10.1016/j.clet.2020.100014.
[37] J.M. Medina, M.I.S. de Rojas, I.F. Sáez Del Bosque, M. Frías, C. Medina, Sulfate resistance in cements bearing bottom ash from biomass-fired electric power plants, Appl. Sci. 10 (2020) 1–11, https://doi.org/10.3390/app10248982.
[38] B. Lothenbach, E. Bernard, U. Mäder, Zeolite formation in the presence of cement hydrates and albite, Phys. Chem. Earth 99 (2017) 77–94, https://doi.org/10.1016/j.pce.2017.02.006.
[39] J. Pokorný, M. Pavlíková, M. Záleská, P. Rovnaníková, Z. Pavlík, Coagulated silica - A-SiO2 admixture in cement paste, in: AIP Conf Proc, American Institute of Physics Inc, 2016, https://doi.org/10.1063/1.4955254.
[40] Environmental Protection Agency US, Protection of Environment Chapter I, 1993.
[41] Standards Australia International., Composts, soil conditioners and mulches., Standards Australia International, 2003..
[42] O. Onuaguluchi, and Ö. Eren, Copper tailings as a potential additive in concrete: consistency, strength and toxic metal immobilization properties, 2012.
[43] F. Vargas, M. Lopez, L. Rigamonti, Environmental impacts evaluation of treated copper tailings as supplementary cementitious materials, Resour. Conserv Recycl 160 (2020), https://doi.org/10.1016/j.resconrec.2020.104890.
[44] J. Smuda, B. Dold, J.E. Spangenberg, K. Friese, M.R. Kobek, C.A. Bustos, H. R. Pfeifer, Element cycling during the transition from alkaline to acidic environment in an active porphyry copper tailings impoundment, Chuquicamata, Chile, J. Geochem Explor 140 (2014) 23–40, https://doi.org/10.1016/j.gexplo.2014.01.013.
[45] K. Scrivener, R. Snellings, and B. Lothenbach, A practical guide to microstructural analysis of cementitious materials, 1st ed., 2016.
[46] A. Madadi, J. Wei, Characterization of calcium silicate hydrate gels with different calcium to silica ratios and polymer modifications, Gels 8 (2022), https://doi.org/10.3390/gels8020075.
[47] J.H. Ideker, K.L. Scrivener, H. Fryda, B. Touzo, Calcium aluminate cements, in: Lea's Chemistry of Cement and Concrete, Elsevier, 2019, pp. 537–584, https://doi.org/10.1016/B978-0-08-100773-0.00012-5.
[48] M. Katsioti, N. Patsikas, P. Pipilikaki, N. Katsiotis, K. Mikedi, M. Chaniotakis, Delayed ettringite formation (DEF) in mortars of white cement, Constr. Build. Mater. 25 (2011) 900–905, https://doi.org/10.1016/j.conbuildmat.2010.06.095.
[49] ASTM International, Standard test method for corrosion potentials of uncoated reinforcing steel in concrete. ASTM C876 - 15. G01.14, *ASTM International*. (2015) 1–8. doi:10.1520/C0876–15.2..
[50] X.R. Nóvoa, Electrochemical aspects of the steel-concrete system. A review, J. Solid State Electrochem. 20 (2016) 2113–2125, https://doi.org/10.1007/s10008-016-3238-z.
[51] C. Andrade, L. Soler, X.R. Novoa, Advances in electrochemical impedance measurements in reinforced concrete, Mater. Sci. Forum 192–194 (1995) 843–856, doi:10.4028/www.scientific.net/msf.192-194.843.
[52] Y.A. Meyer, I. Menezes, R.S. Bonatti, A.D. Bortolozo, W.R. Osório, EIS Investigation of the corrosion behavior of steel bars embedded into modified concretes with eggshell contents, Met. (Basel) 12 (2022) 417, https://doi.org/10.3390/met12030417.
[53] J. Shi, X. Guan, J. Ming, X. Zhou, Improved corrosion resistance of reinforcing steel in mortars containing red mud after long-term exposure to aggressive environments, Cem. Concr. Compos 130 (2022) 104522, https://doi.org/10.1016/j.cemconcomp.2022.104522.
[54] J. Shi, M. Wu, J. Ming, Long-term corrosion resistance of reinforcing steel in alkali-activated slag mortar after exposure to marine environments, Corros. Sci. 179 (2021), https://doi.org/10.1016/j.corsci.2020.109175.
[55] G. Feng, Z. Jin, Y. Jiang, X. Wang, D. Zhu, Localized corrosion propagation of steel in cracked mortar and long-term corrosion of steel reinforcement in cracked concrete in seawater environment, Corros. Sci. 228 (2024), https://doi.org/10.1016/j.corsci.2023.111793.
[56] J.B. Jorcin, M.E. Orazem, N. Pébère, B. Tribollet, CPE analysis by local electrochemical impedance spectroscopy, : Electro Acta (2006) 1473–1479, https://doi.org/10.1016/j.electacta.2005.02.128.
[57] O. Gharbi, A. Dizon, M.E. Orazem, M.T.T. Tran, B. Tribollet, V. Vivier, From frequency dispersion to ohmic impedance: A new insight on the high-frequency impedance analysis of electrochemical systems, Electro Acta 320 (2019), https://doi.org/10.1016/j.electacta.2019.134609.
[58] H. Liu, X. Lyu, Y. Zhang, G. Luo, W. Li, Steel corrosion evaluation of basalt fiber rpc affected by crack and steel-concrete interface damage using electrochemical methods, Sensors 20 (2020) 1–16, https://doi.org/10.3390/s20185027.
[59] C. Andrade, M. Keddam, X.R. Nóvoa, M.C. Pérez, C.M. Rangel, H. Takenouti, Electrochemical behaviour of steel rebars in concrete: influence of environmental factors and cement chemistry, Electro Acta 46 (2001) 3905–3912, https://doi.org/10.1016/S0013-4686(01)00678-8.

[60] X.R. Nóvoa, Electrochemical aspects of the steel-concrete system. A review, J. Solid State Electrochem. 20 (2016) 2113–2125, https://doi.org/10.1007/s10008-016-3238-z.
[61] J.A. Gonzalez, A. Molina, M.L. Escudero, and C. Andradet, Errors in the electrochemical evaluation of very small corrosion rates. Polarization resistance method applied to corrosion of steel in concrete, 1985.
[62] G. Liu, Y. Zhang, M. Wu, R. Huang, Study of depassivation of carbon steel in simulated concrete pore solution using different equivalent circuits, Constr. Build. Mater. 157 (2017) 357–362, https://doi.org/10.1016/j.conbuildmat.2017.09.104.